DOI: 10.13009/EUCASS2017-589

Numerical Simulation of Turbulent Boundary Layers with Foreign Gas Transpiration using OpenFOAM

Daniel Prokein and Jens von Wolfersdorf
Institute of Aerospace Thermodynamics (ITLR), University of Stuttgart
Pfaffenwaldring 31, 70569 Stuttgart, Germany

Abstract

Transpiration cooling in combination with porous high-temperature materials is a promising technique for thermal protection of highly-loaded aerospace applications. In this study, we present a modified OpenFOAM solver which is applied to the simulation of a turbulent channel flow with boundary layer blowing. Same and foreign gas injection is simulated for cold and heated main flow conditions and the results are compared to experimental data and correlations from literature. A very good overall agreement is found for velocity and temperature boundary layer profiles as well as the dimensionless parameters for wall shear stress and heat transfer.

1. Introduction

Thermal protection systems are of great importance for many aerospace applications involving high thermal loads on the applied materials. Examples such as rocket combustion chambers, reentry heat shields or scramjet applications clearly illustrate the demand for reliable and efficient protection techniques. Even though modern high-temperature materials keep pushing the temperature limits towards higher levels, active cooling is still necessary for structures exposed to extreme thermal conditions. This is especially applicable if reusability comes into focus or the foreseen mission profiles involve long-duration exposure to high heat fluxes. An interesting candidate for the thermal protection of such applications is transpiration cooling in combination with porous high-temperature materials. Although the great potential of transpiration cooling has been recognized long ago [1], the lack of suitable materials has prevented a wide application up to today. However, recent progress in the field of material sciences has led to the availability of modern porous materials such as ceramic matrix composites (CMC) [2] and thus triggered new interest into this technology. While different experiments [3-5] successfully demonstrated the general feasibility of aerospace applications involving transpiration-cooled CMCs, also the physical modelling of the cooling technique is challenging and an active topic of research. With respect to this, especially the development of numerical tools is of great importance for the efficient and reliable design of future applications.
In general, transpiration cooling is based on two mechanisms which are schematically illustrated in figure 1. First, the exchange of energy while a coolant gas is flowing through the hot porous material and second, the injection of cool fluid into the boundary layer which decreases the effective heat load onto the structure. Likewise, the modelling approaches can be divided into studies focusing on the internal [6-8] or external processes [9-13]. Since both effects interact with each other, a conjugate problem arises.

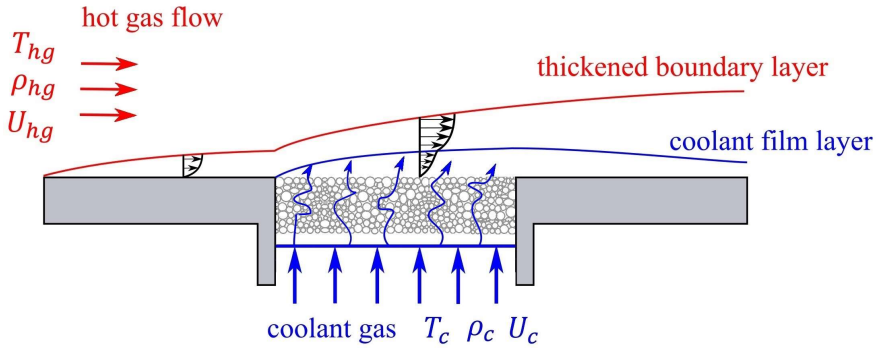

Figure 1: Schematic illustration of transpiration cooling.

DOI: 10.13009/EUCASS2017-589

At ITLR, we are developing a computational fluid dynamics (CFD) solver based on the OpenFOAM environment which shall be able to simulate the complete problem of transpiration cooling. At first, a volume-averaged porous structure solver has been developed for simulation of the internal cooling and through-flow behaviour, see Prokein et al. [14]. In a second step, the numerical simulation of the external cooling mechanism has been investigated and is presented in this report. Many early experimental studies explored the influence of transpiration cooling for sub- and supersonic main flows, e.g. Leadon and Scott [15], Rubesin [16] and Moffat and Kays [10]. A strong reduction in skin friction and heat transfer for boundary layer blowing was detected which can be correlated to the dimensionless blowing parameter defined as:

$$F = \frac{\rho_c U_c}{\rho_{hg} U_{hg}} = \frac{\dot{m}_c / A_c}{\dot{m}_{hg} / A_{hg}} = \frac{\text{transpired mass flux}}{\text{hot gas mass flux}} \quad , \tag{1}$$

where ρ is density, U is velocity and $\dot{m}/A$ denotes the area-specific mass flow rate. The subscripts 'c' and 'hg' represent values for coolant or hot gas flow, respectively. Several analytical correlations have been deduced from the existing experimental data in order to predict skin friction coefficient and Stanton number for transpired surfaces.
Landis and Mills [19], Kays et al. [18] and more recently Meinert et al. [9] additionally investigated the influence of foreign gas injection using various light and heavy coolant gases. This aspect is especially interesting with respect to the underlying application-driven motivation. As an example, a potential transpiration-cooled combustion chamber would presumably make use of the already available fuel as coolant fluid. A substantial effect of the properties of the transpirant on the boundary layer characteristics was found by all investigations which can be considered by introducing fluid-dependent correction factors into the correlations. Kays et al. [18] proposed the following relations for the ratios of skin friction coefficient and Stanton number with and without blowing of arbitrary coolant gases:

$$\frac{C_f/2}{(C_f/2)_0} = \frac{b_f}{e^{b_f} - 1} \quad \text{with} \quad b_f = \frac{F}{(C_f/2)_0}\, k_M \tag{2}$$

and

$$\frac{St}{St_0} = \frac{b_h}{e^{b_h} - 1} \quad \text{with} \quad b_h = \frac{F}{St_0}\, k_T^*\, k_M^*\, k_C^* \tag{3}$$

The modified blowing parameters b_f and b_h account for the influence of foreign gas injection. Kays et al. [18] proposed $k_C^* = \left(c_{p,c}/c_{p,hg}\right)^{0.6}$, $k_M = k_M^* = k_T^* = 1$, whereas Meinert et al. [9] determined differing values from fitting their experimental data, i.e. $k_M = \left(M_{hg}/M_c\right)^{0.8}$, $k_C^* = 1$, $k_M^* = \left(M_{hg}/M_c\right)^{0.6}$, $k_T^* \approx (T_{aw}/T_w)^{0.2\ldots0.4}$. Despite of the generally good approximations given by equations (2) and (3), the models are limited to one-dimensional cooling situations and require non-blowing parameter values for C_f and St which are not easy to obtain for complex flow situations. In this regard, CFD offers the opportunity of simulating the complete flow field around arbitrary geometries whilst considering surface transpiration. The injection modelling as well as the coupling of external flow field to porous structure are challenging, though.
The purpose of this work is to validate our numerical solver for the simulation of boundary layer injection with various gases into a cold or heated turbulent main flow. First, the physical modelling of the turbulent channel flow is described which involves the detailed consideration of species transport as well as the calculation of mixture properties for the multicomponent flow. Subsequently, the investigated experimental test case by Meinert [19] and the numerical setup for the corresponding OpenFOAM simulations are presented. Two approaches for injection modelling are explored before the selected model is applied to simulate turbulent channel flow with blowing of Air, Argon and Helium. In addition to isothermal test cases also gas injection for heated main flows is simulated and the results are compared to the experimental data by Meinert [19]. Finally, the influence of boundary layer blowing on skin friction as well as heat transfer is discussed for different coolant gases.

2. Physical modelling of main flow

For our numerical study of a turbulent channel flow, conservation equations for mass, momentum, species and energy have to be solved. A common approach to describe turbulent flows is the Reynolds decomposition into an average and a fluctuating part. For compressible flows with density fluctuation, an additional Favre-averaging simplifies the resulting equations. Although, the here presented test cases do not require non-stationary modelling, the transient conservation equations given in the following are solved until steady-state conditions are reached.

DOI: 10.13009/EUCASS2017-589

2.1 Governing equations

The conservation equations as implemented and solved in the utilized OpenFOAM solver read:

$$\frac{\partial \bar{\rho}}{\partial t} + \nabla \cdot (\bar{\rho}\widetilde{U}) = 0 \tag{4}$$

$$\frac{\partial}{\partial t}(\bar{\rho}\widetilde{U}) + \nabla \cdot (\bar{\rho}\widetilde{U} \otimes \widetilde{U}) = -\nabla \bar{p} + \nabla \cdot (\tilde{\tau}_{eff}) \tag{5}$$

$$\frac{\partial}{\partial t}(\bar{\rho}\widetilde{Y}_i) + \nabla \cdot (\bar{\rho}\widetilde{U}\widetilde{Y}_i) = \nabla \cdot \left(\bar{\rho}\left(D_{12} + \frac{\nu_t}{Sc_t}\right)\nabla \widetilde{Y}_i\right) \tag{6}$$

$$\begin{aligned} &\frac{\partial}{\partial t}(\bar{\rho}\tilde{h}_s) + \nabla \cdot (\bar{\rho}\widetilde{U}\tilde{h}_s) + \frac{\partial}{\partial t}\left(\bar{\rho}\frac{1}{2}|\widetilde{U}|^2\right) + \nabla \cdot \left(\bar{\rho}\widetilde{U}\frac{1}{2}|\widetilde{U}|^2\right) - \frac{\partial \bar{p}}{\partial t} \\ &= \nabla \cdot \left(\bar{\rho}\left(\alpha + \frac{\nu_t}{Pr_t}\right)\nabla \tilde{h}_s\right) + \nabla \cdot \left[\bar{\rho}\left(D_{12} + \frac{\nu_t}{Sc_t} - \alpha - \frac{\nu_t}{Pr_t}\right)(\tilde{h}_{s1} - \tilde{h}_{s2})\,\nabla \widetilde{Y}_1\right] + \nabla \cdot (\tilde{\tau}_{eff} \cdot \widetilde{U}) \end{aligned} \tag{7}$$

In equations (4) to (7), U represents the velocity vector, ρ and p denote fluid density and pressure, Y_i is the species mass fraction, α the thermal diffusivity, and h_s is the sensible enthalpy. The effective stress tensor $\tilde{\tau}_{eff}$ comprises of viscous and turbulent stresses. An additional term accounting for energy transport due to mass diffusion is added to the standard sensible enthalpy equation as discussed in chapter 2.4. Turbulent transport of momentum is calculated based on the eddy viscosity ν_t which is determined through the applied turbulence model as described in the following section. Assuming a constant turbulent Prandtl number of $Pr_t = 0.87$ (see also [19]), the turbulent thermal diffusivity can be determined from $\alpha_t = \nu_t / Pr_t$. Likewise, turbulent mass transport due to diffusion is considered by $D_{12,t} = \nu_t / Sc_t$ with a constant turbulent Schmidt number of $Sc_t = 0.8$. The applied value has been found to give reasonable agreement in turbulent channel flow experiments of Dunbar and Squire [20] and is also suggested by Landis and Mills [17].

2.2 Turbulence modelling

For turbulence modelling the Shear Stress Transport model as described by Menter [21] is selected. The model formulation combines two widely used turbulence models, namely the $k-\varepsilon$ model proposed by Launder and Sharma [22] and the $k-\omega$ model developed by Wilcox [23]. Both of the models are well validated but exhibit certain strengths and weaknesses depending on the considered flow situation. The $k-\omega$ model is able to predict turbulence more accurately near surfaces leading to an improved calculation of wall shear stress and heat transfer. In contrast to this, the model shows a strong sensitivity to free-stream values of ω outside the boundary layer, where turbulent behaviour is better resolved by the $k-\varepsilon$ model. In order to combine the advantages of both models, Menter [21] suggested the SST model which incorporates a blending function that activates the $k-\omega$ model in wall-near regions and the $k-\varepsilon$ formulation further away from the wall. From the solution of the two resulting conservation equation, the turbulent eddy viscosity ν_t is calculated. A detailed description of the SST turbulence model as well as the mathematical formulation are given in references [21] and [24].

2.3 Thermophysical modelling

For the here presented simulations with foreign gas injection we consider a binary mixture of Helium or Argon (denoted by the variable index 1) and the main flow of Air (index 2). In the following, the origin of thermophysical properties used in the numerical simulations is explained. At first, the way of determining the physical properties of the pure gases is given. Afterwards, the applied mixture laws are discussed.
The specific heat capacity of pure gases at a wide temperature range can be calculated from the JANAF/NASA polynomials [25]:

$$\frac{c_p}{R_s} = a_1 + a_2 T + a_3 T^2 + a_4 T^3 + a_5 T^4 \quad , \tag{8}$$

where R_s is the specific gas constant of the considered gas and a_1 to a_5 are fluid-dependent coefficients.

DOI: 10.13009/EUCASS2017-589

Dynamic viscosities of pure gases are calculated according to Sutherland's law [26]:

$$\mu = \frac{A_s \sqrt{T}}{1 + \frac{T_s}{T}} \quad , \tag{9}$$

where A_s and T_s are the Sutherland constants as given in table 1, see also White [27].
From the dynamic viscosity μ, the specific gas constant R_s and the specific heat capacity at constant volume c_v, the thermal conductivity λ is then determined by means of the modified Eucken correlation for polyatomic gases [28]:

$$\frac{\lambda}{\mu\, c_v} = 1.32 + \frac{1.77}{c_v/R_s} \quad . \tag{10}$$

Having the thermophysical properties of the pure gases available, the properties of Helium-Air or Argon-Air mixtures can be determined according to mixing laws. Although Air itself is a mixture of various gases (e.g. nitrogen, oxygen, Argon, carbon dioxide and others), it is treated as a pure gas by our OpenFOAM solver. All necessary coefficients are provided directly for Air and have been obtained either through experiments with Air or respective mixture calculations. The specific enthalpy h_{mix} and heat capacity $c_{p,mix}$ of mixtures are easily obtained from weighting with the species mass fractions Y_i, i.e.

$$h_{mix} = \sum_i Y_i\, h_i \qquad \text{and} \qquad c_{p,mix} = \sum_i Y_i\, c_{p,i} \quad . \tag{11), (12}$$

For the dynamic viscosity, Sutherland [26] and Wilke [29] suggested the following equation for mixtures of non-polar gases at low-pressures:

$$\mu_{mix} = \sum_{i=1}^{n} \frac{\mu_i}{1 + \frac{1}{\psi_i} \sum_{\substack{j=1 \\ j \neq i}}^{n} \psi_j \Phi_{ij}} \qquad \text{with} \qquad \Phi_{ij} = \left[1 + \left(\frac{\mu_i}{\mu_j}\right)^{\frac{1}{2}} \left(\frac{M_j}{M_i}\right)^{\frac{1}{4}}\right]^2 \left[8\left(1 + \frac{M_i}{M_j}\right)\right]^{-\frac{1}{2}} \quad , \tag{13}$$

where ψ_i denotes the molar fraction of species 'i' and Φ_{ij} is an interaction parameter calculated from the molecular weights M_i and the dynamic viscosities μ_i. Wilke's law has been extensively tested by many authors who found an accuracy of better than 2% when compared to experimental values, see for example Wilke [29] or Dean and Stiel [30].
Likewise, Wassiljewa [31] introduced a mixture rule to obtain the thermal conductivity of a gas mixture in 1904. Her findings were later examined by Mason and Saxena [32] who proposed the corresponding interaction parameter A_{ij}. The combination yields:

$$\lambda_{mix} = \sum_{i=1}^{n} \frac{\lambda_i}{1 + \frac{1}{\psi_i} \sum_{\substack{j=1 \\ j \neq i}}^{n} \psi_j A_{ij}} \qquad \text{with} \qquad A_{ij} = \varepsilon \cdot \left[1 + \left(\frac{\lambda_{tr,i}}{\lambda_{tr,j}}\right)^{\frac{1}{2}} \left(\frac{M_i}{M_j}\right)^{\frac{1}{4}}\right]^2 \left[8\left(1 + \frac{M_i}{M_j}\right)\right]^{-\frac{1}{2}} \quad . \tag{14}$$

The interaction parameter A_{ij} is determined from the molecular weights M_i, the monoatomic values of the thermal conductivities $\lambda_{tr,i}$ and the factor ε near unity. Different values were found by Mason and Saxena ($\varepsilon = 1.065$) and later Tandon and Saxena ($\varepsilon = 0.85$). Poling et al. [28] suggest a value of $\varepsilon = 1.0$ which is also employed in our study. In combination with the relation $\lambda_{tr,i}/\lambda_{tr,j} = (\mu_i/\mu_j)\left(M_j/M_i\right)$, this leads to $A_{ij} = \Phi_{ij}$, so that the previous viscosity interaction parameter is applied for both viscosity and thermal conductivity calculation. Poling et al. report a general error of less than 3 to 4% for non-polar gas mixtures.

2.4 Modelling of species transport

The diffusion law describes the dependency of the diffusion flux vector $\vec{j}$ from species concentration and temperature, see for example Schlichting and Gersten [34], Sparrow et al. [35] or Anderson [36]. For the first component of a binary mixture (subscript '1') it reads

$$\vec{j}_1 = -\rho D_{12} \left[\nabla Y_1 + \bar{\alpha}\, Y_1 (1 - Y_1)\, \nabla(\ln(T))\right] \quad . \tag{15}$$

The first term determines diffusion due to concentration gradients and is also known as Fick's diffusion law. The second term describes thermal diffusion because of temperature gradients. In equation (15) diffusion due to pressure gradients and volume forces has been neglected. Both effects do not play a significant role within the boundary layer and at the absence of a force field other than the gravity field [34-36]. Moreover, thermal diffusion is neglected by

DOI: 10.13009/EUCASS2017-589

assuming $\bar{\alpha} = 0$. For transpiration cooling this simplification is justified as the diffusion is primarily governed by concentration gradients and convective mixing processes [18]. With the made assumptions, Fourier's law for a binary non-reacting gas mixture is modified to

$$\vec{q} = -\lambda \nabla T + (h_1 - h_2)\, \vec{j}_1 \quad . \tag{16}$$

The first term represents heat conduction, whereas the second term accounts for energy transport due to molecular diffusion. The latter mechanism introduces an additional term in the enthalpy balance (see equation (7)) which may have a significant contribution if the Lewis number $Le = Sc/Pr$ is not equal to unity and the difference between the specific heat capacities of the considered species is large.
The binary diffusion coefficient D_{12} has the units m^2/s and can be calculated according to the Fuller-Schettler-Giddings relation as defined by [37]:

$$D_{12} = D_{AB} = \frac{0.0101325\ T^{1.75}\left({}^{1}/_{M_A} + {}^{1}/_{M_B}\right)^{0.5}}{p\left\{\left(\sum_A v_i\right)^{1/3} + \left(\sum_B v_i\right)^{1/3}\right\}^2} \quad \left[\frac{\mathrm{m}^2}{\mathrm{s}}\right] \quad , \tag{17}$$

with temperature T [K], pressure p [Pa], molar mass M [kg/kmol] and diffusion volumes v_i [cm^3]. The relation was obtained by a least-square analysis of diffusion experiments on various binary systems. The authors deduced diffusion volumes for several atoms and simple molecules as included for Air, Argon and Helium in table 1. Fuller and Giddings [38] compared the accuracy of different methods to predict gaseous diffusion coefficients and found an average deviation of 4.2% from experimental data for the relation given in equation (17).

Table 1: Selected fluid properties of Air, Argon and Helium [27,37]

	$M\ \left[\frac{kg}{kmol}\right]$	$A_s\ \left[\frac{kg}{m\,s\,\sqrt{K}}\right]$	$T_s\ [K]$	$\sum v_i\ [cm^3]$
Air	28.916	$1.460846 \cdot 10^{-6}$	111	19.7
Helium	4.003	$1.460689 \cdot 10^{-6}$	79.44	2.67
Argon	39.948	$1.964495 \cdot 10^{-6}$	144	16.2

3. Test case description

For the validation of our modified OpenFOAM solver we selected a subsonic turbulent channel flow with foreign gas blowing as a validation test case. The choice of the test case is motivated by an experimental study of Meinert. In his work, the author performed various boundary layer blowing experiments at the TU Dresden and provides selected data on velocity and temperature profiles in reference [19]. A brief account on Meinert's experiments as well as the description of our numerical setup for the OpenFOAM simulations are given in the following.

3.1 Experiment

In the considered wind tunnel experiments a blower supplied a continuous flow of heated Air of up to $\dot{m}_{hg} = 1.3\ \mathrm{kg/s}$ and $T_{hg} \approx 300\ °\mathrm{C}$. The static pressure in the test section was around 1 bar, hot gas velocities could be adjusted to values of up to $U_{hg} = 160\ \mathrm{m/s}$. The measurement section has a constant cross section of 114 mm width and 100 mm height. At the entrance of the segment, the existing boundary layer is removed by boundary layer suction ($x = 0$). Thus, a new boundary layer is building up which is tripped artificially by a tripping device installed 100 mm downstream of the suction blade. Between the axial positions $200\ \mathrm{mm} < x < 470\ \mathrm{mm}$, the wall is replaced by a porous wall segment made from stainless steel packed bed material (SIKA-R5) with a porosity of 30% and an average pore diameter of 10 µm. With respect to the average pore diameter, SIKA-R5 compares well to modern CMC materials such as C/C which exhibit an average crack size of $11 - 14\ \mu\mathrm{m}$ [39]. The porosity of CMC materials, e.g. ~15% for C/C, is generally lower, though. Coolant gases such as Air, Argon and Helium are supplied via gas bottles and mass flow controllers to the coolant reservoir below the porous wall segment. For measuring the boundary layer profiles a combined sensor containing a static pressure probe, a miniature pitot probe and a miniature thermocouple was utilized. Measurements were taken in the middle of the channel, the sensors wall distance was adjusted by a precise positioning system in order to traverse the boundary layer. Evaluation positions for the here discussed boundary layer profiles were measured at the positions $x = 342\ \mathrm{mm}$ or $x = 442\ \mathrm{mm}$. Moreover, the wall

DOI: 10.13009/EUCASS2017-589

temperature on the porous sample was determined by an infrared pyrometer. All measurements were done for steady-state conditions, i.e. when thermal equilibrium was reached. The resulting test conditions correspond to channel Reynolds numbers Re_x between $1 \cdot 10^6$ and $3 \cdot 10^6$. Meinert [9] points out that the evaluation of measured data for foreign gas transpiration is challenging due to the strong density variations in the boundary layer. Velocity profiles are calculated via Wuest's formula [40] from the measured dynamic pressure. As concentration profiles were not measured in the experiments, a simplified analogy of momentum transport and diffusion in the turbulent boundary layer was employed in order to determine the required fluid properties of the binary gas mixtures.
More information on the experimental setup and the applied data analysis methods can be found in references [9,19].

3.2 Numerical setup

For the simulation of turbulent channel flow with foreign gas injection a modified OpenFOAM solver for non-reactive, multi-component flows has been developed. The pressure-based solver is built upon rhoReactingFOAM which comes with the standard repository of OpenFOAM (release 2.3.x). The transient solver utilizes the "Pressure Implicit with Splitting of Operators (PISO)" algorithm [41, 42] for pressure-velocity coupling and requires Courant-Friedrich-Lewy (CFL) numbers smaller than unity. Despite of the transient formulation, the solver is run until quasi steady-state is reached to enable a comparison to the measurements. Several modifications were introduced to the solver which mainly focus on the thermophysical modelling of gas mixtures and the species transport. Mixing laws for viscosity and thermal conductivity as described in chapter 2.3 were implemented. Moreover, the described modelling of the diffusion coefficient according to the Fuller-Schettler-Giddings relation has been supplemented and the species transport as well as the energy equation were adapted to the form given in equations (6) and (7).
A two-dimensional numerical grid consisting of around 200,000 rectangular cells represents the turbulent channel in the numerical simulations. The channel walls are assumed as fully turbulent, i.e. no laminar-turbulent transition is taken into account. Turbulence modelling is done by means of the Low-Re-formulation of the shear stress transport model by Menter et al. [24]. The inlet conditions were prescribed with $TI = 2\%$ for the turbulent kinetic energy and a mixing length of $L_{t,in} = 4.8\% \cdot d_{hyd}$ for the calculation of the specific dissipation rate. For a good approximation of turbulent behaviour close to the channel wall, a dimensionless wall distance of $y_1^+ < 1$ was obeyed during mesh generation. The computational domain with the applied boundary conditions is shown in figure 2. An Air flow with constant area-specific mass flux and constant static temperature is prescribed at the inlet, whereas the outlet is modelled by a constant pressure boundary condition of $p = 10^5$ Pa. For the isothermal test cases the walls are set to be adiabatic, whereas for the heated test cases the experimentally measured temperature is imposed at the porous wall. Since no experimental data on the wall temperature up- and downstream of the porous segment is available, the surface temperature measured on the porous wall for the no-blowing case is applied at these positions. For all cases, the coolant gas is injected with the measured wall temperature T_w, i.e. thermal equilibrium is assumed at the outflow boundary of the porous wall segment. The modelling of coolant injection is described in detail in the next chapter.

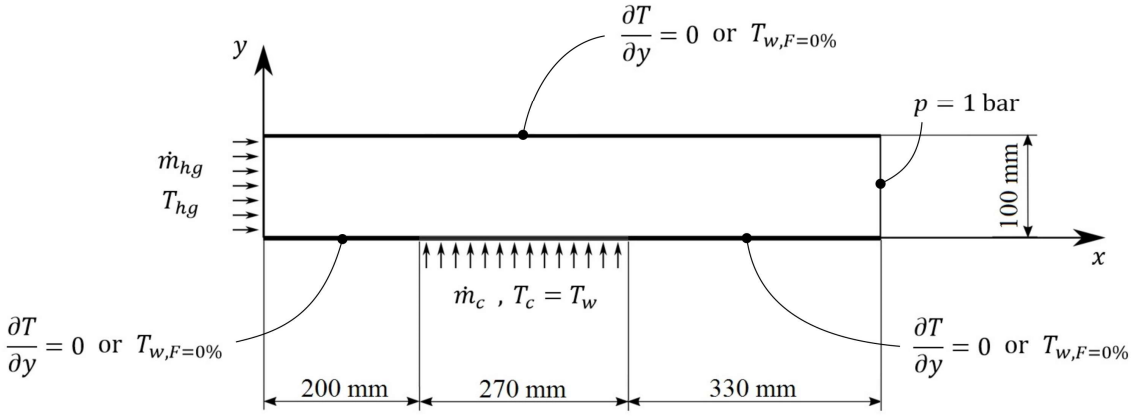

Figure 2: Computational domain and applied boundary conditions for the selected test case.

DOI: 10.13009/EUCASS2017-589

4. Injection modelling

One of the main questions when modelling transpiration cooling is how to inject the coolant fluid into the hot gas boundary layer. With respect to the considered test case, the transpired channel wall does consist of both components, fluid (pores) as well as solid (struts). Both phases interact differently with an overflowing gas. At a solid interface, the no-slip condition applies which results in a zero-velocity and a decrease of momentum in the boundary layer close to the wall. On the other hand, the coolant fluid located at a pore position cannot sustain shear stress.
In general, porous materials applied for thermal protection systems in aerospace exhibit rather dense structures with open porosities below 35% and microscopic pore sizes of a few micrometres. If the pores are to be resolved individually, very large numerical grids are required. Thus, this approach is not practical for the numerical simulation of an application-sized porous structure. Similar to the volume-averaged modelling approach employed for the simulation of the porous material's internal structure such as described in [14], we investigated the applicability of two surface-averaging injection models. Both approaches do not exactly reproduce the pore resolution but model the coolant injection on a larger scale. Figure 3 schematically illustrates the approaches which are called "discrete pores model" and "continuous blowing model" in the following.

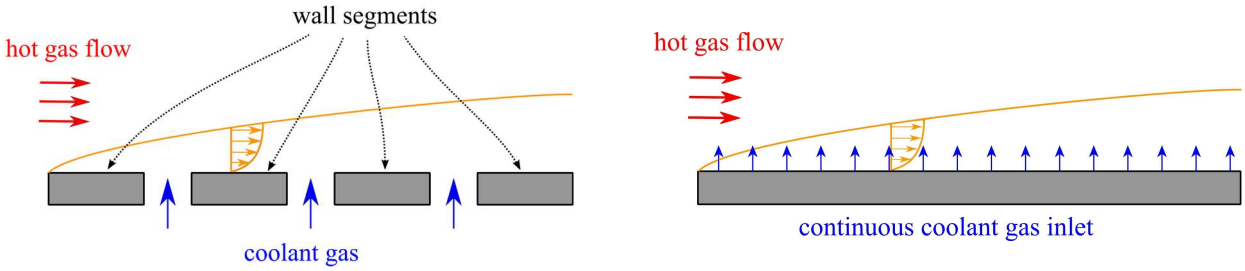

Figure 3: Macroscale modelling approaches for gas injection through porous walls with microscopic pores: Discrete pores model and continuous blowing model.

As can be seen from the figure, the discrete pores model represents a porous wall by a series of enlarged holes and wall segments distributed according to the material's porosity. Holes are numerically modelled as inlets, whereas the wall segments are treated as common wall patches. Thus, this model naturally inherits fluid and solid wall properties, even though the pore resolution is not met. Our test case exhibits a porous wall segment made from SIKA-R5 with a length of 270 mm and 30% open porosity. The wall segment corresponds to around 8100 pores of 10 µm size in average. For our numerical model we choose two rather rough representations with 9 and 27 pores for the considered porous wall. The pore resolution indicating the model's resolution with respect to the real material is thus 1:900 and 1:300, respectively. As shown in the sketch, sequences of pore and wall are distributed regularly. The second considered modelling approach uses a single numerical patch for the complete porous wall. The coolant mass flow is evenly distributed over the surface resulting in a continuously transpiring wall segment. The influence of the solid struts of the porous wall is modelled by the applied boundary conditions, i.e. $U_x = 0$, $U_y = \dot{m}_C/(\rho_c\, A_C)$, $k = 0$ and $\omega_{SST} = (6\nu_w)/(0.075\, \Delta y^2)$.
For a comparison of the injection models we use the described test case of a turbulent channel flow with an Air injection of $F = 0.5206\%$ at isothermal conditions. The numerical results are compared to experimental data by Meinert [19]. Figure 4 shows contour plots of the axial velocity for the three injection cases. The detail views illustrates the flow behaviour at the beginning of the porous wall segment ($180\ \text{mm} < x < 260\ \text{mm}$) up to a wall distance of around 5 mm. A zoom factor of five is used on the y-axis for better illustration. The coolant inlet positions are clearly visible for the discrete pores model, whereas the injection is uniform and at lower velocity magnitude for the continuous blowing model. The jet-like injections for the pore models disturb the boundary layer development as shown by the wave-like variation of velocity isolines. Although this is visible for both pore resolutions, the increase of pores has a smoothing effect.

DOI: 10.13009/EUCASS2017-589

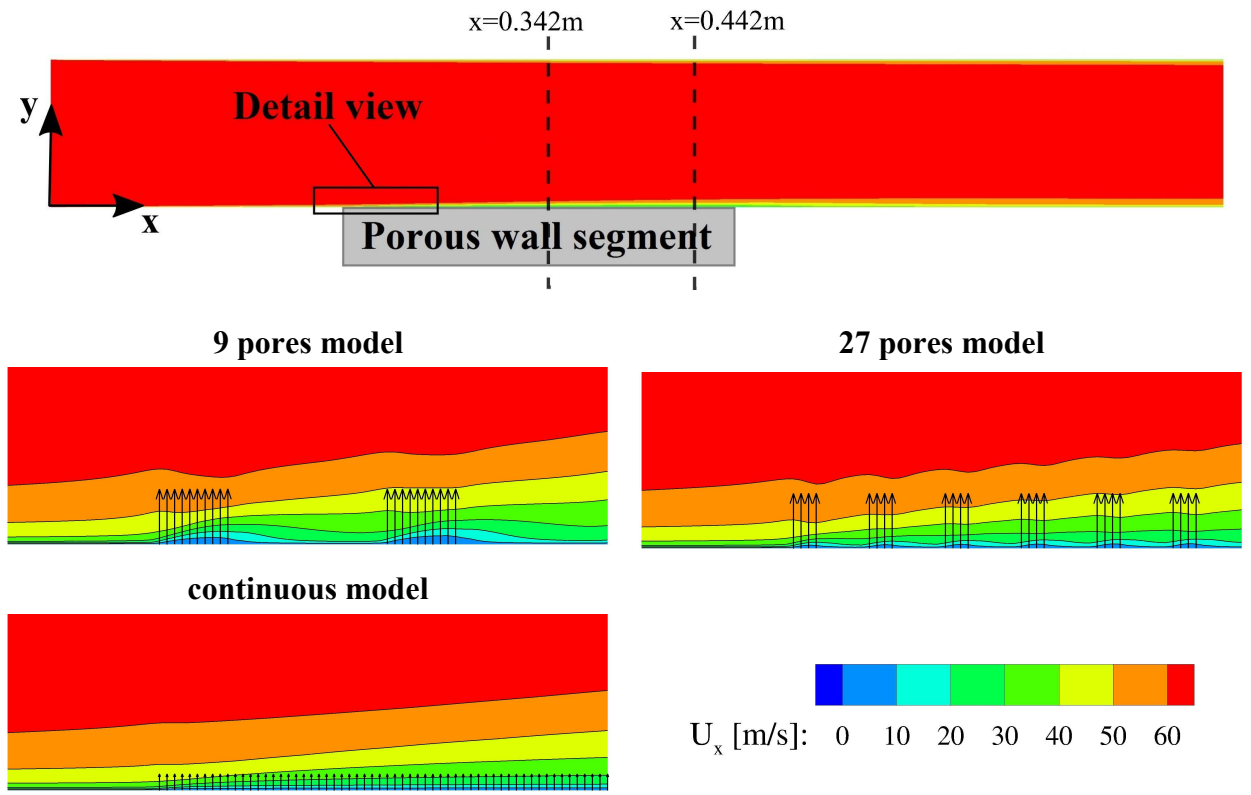

Figure 4: Detail view of velocity contour plot around injection area, i.e. 180 mm $< x <$ 260 mm. For the sake of clarity, the detail view's axes size was scaled by ratio $y : x = 5 : 1$.

In figure 5 the velocity profiles at $x = 442$ mm for the simulations of the three cases are compared to experimental data. A good agreement is found between experiment and simulation for both injection models. The detail view on the right-hand side of figure 5 reveals a smaller deviation for the continuous blowing model close to the wall when compared to the discrete model. Moreover, the model better reproduces the smooth velocity profile found in the measurements. Comparing the two pore resolutions for the discrete model, we find a minor improvement for the higher resolution which is also closer to the continuous model's results.

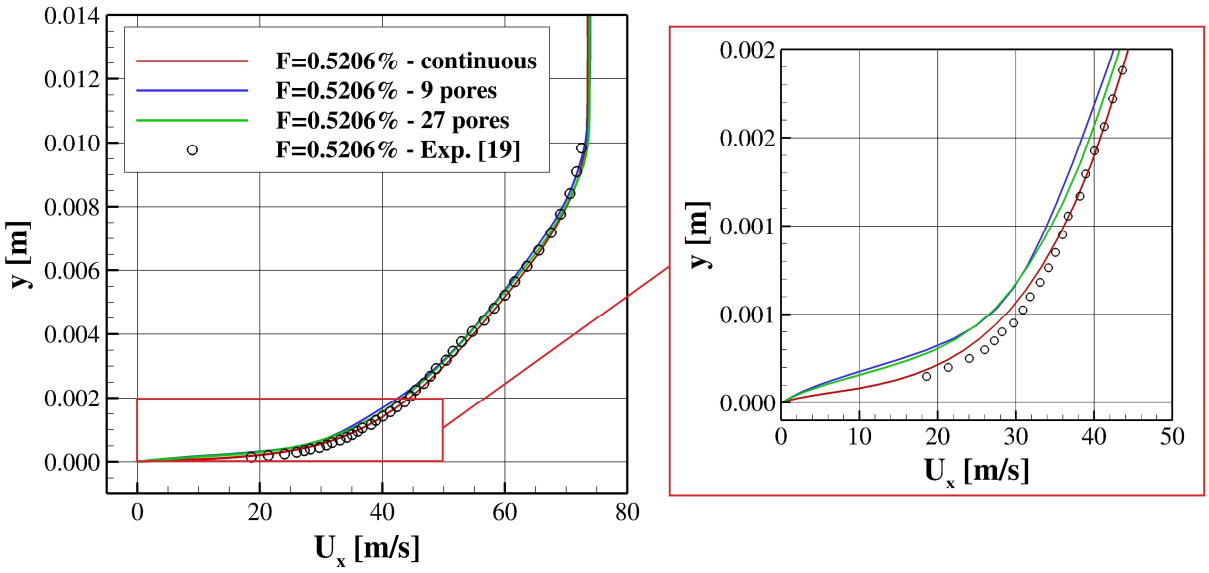

Figure 5: Velocity distribution over wall distance for discrete pores model (9 and 27 pores) and continuous blowing model at axial position $x = 0.442$ m. Right hand side diagram shows a detail view.

DOI: 10.13009/EUCASS2017-589

In addition to the velocity profiles, the skin friction coefficient over channel length was calculated from

$$\frac{C_{fx}}{2} = \frac{\tau_{w,x}}{\rho_\infty U_{x,\infty}^2} = \frac{\mu_w \left.\frac{\partial U_x}{\partial y}\right|_{w,x}}{\rho_\infty U_{x,\infty}^2} \quad , \tag{18}$$

where $\tau_{w,x}$ denotes the local wall shear stress. Equation (18) was evaluated for the complete porous patch, disregarding of the conflicting definition of wall shear stress for a fluid pore. The resulting distribution of the skin friction coefficient over the streamwise coordinate is given in figure 6. The physical findings such as the strong decrease of wall shear stress for boundary layer blowing will be discussed in more detail later. For the here presented comparison of injection models it is important to note the fluctuating values for the discrete pores models around the uniform distribution for the continuous blowing model. With each pore / wall sequence the skin friction coefficient steeply decreases and rises, respectively.

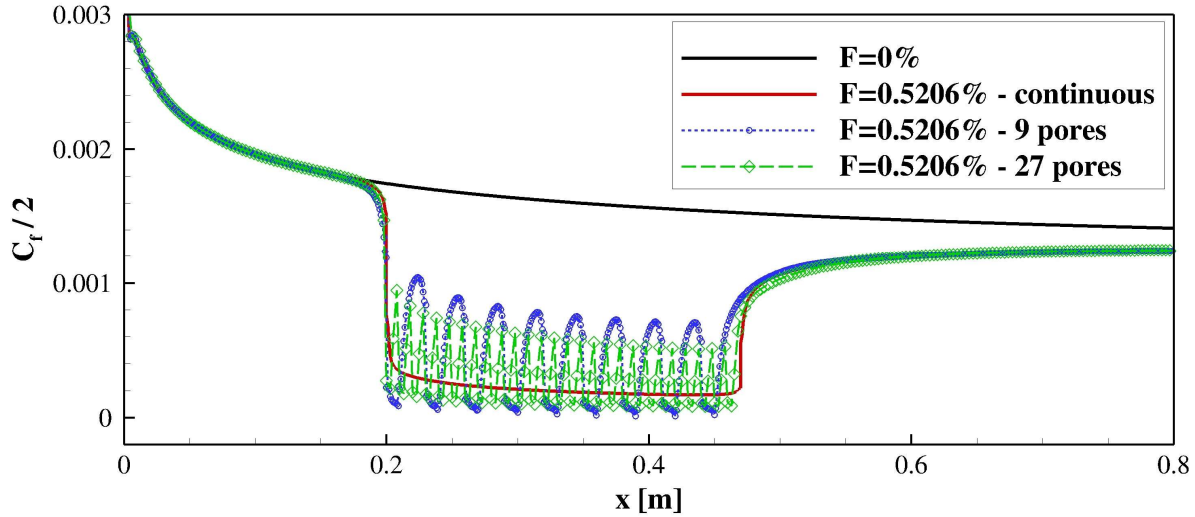

Figure 6: Distribution of skin friction coefficient over channel length for discrete pores and continuous blowing model. Air injection into main flow at isothermal conditions.

From the injection modelling investigation, we can conclude that both investigated approaches were successfully applied to our test case and show a good agreement with the velocity profile measured at $x = 442$ mm of the considered turbulent channel. Regarding the skin friction coefficient, the discrete pores model shows strong variations over the sample surface. This is due to the jet-like mass injections which lead to velocity fluctuations in the boundary layer. The consequent dependency of the results on the evaluation position as well as the intricate mesh generation are disadvantages when compared to the continuous blowing model.
Based on the discussed results the continuous blowing model was selected for all further investigations presented in this study.

5. Numerical results

In the following section numerical results for the selected test case of a turbulent channel flow with boundary layer blowing are presented. Air, Argon and Helium were injected for the isothermal cases, i.e. main flow and transpired gas are at the same temperature. For the heated main flow cases only the results for Argon and Helium were compared to experimentally measured boundary layer profiles due to the availability of experimental data. Finally, the dimensionless parameters C_f and St for wall shear stress and wall heat flux are determined from the numerical results and plotted against correlations from literature.

5.1 Injection of Air at isothermal conditions

At first, the injection of Air into a main flow of the same species was simulated at isothermal conditions, i.e. $T_{hg} = T_c = 293.15$ K. At the considered Mach number of around 0.2, this corresponds to an incompressible flow

DOI: 10.13009/EUCASS2017-589

situation. Figure 7 gives velocity distributions over wall distance with varying blowing parameter for simulation and experiment. The case of no injection ($F = 0\%$) was evaluated at a different axial position, i.e. $x = 342$ mm, when compared to the other measurements ($x = 442$ mm). As the porous wall insert is located from 200 mm to 470 mm, the measurements were taken at the middle and close to the rear edge of the sample, see also figure 4. The simulation of the no blowing case was used as a reference case for the determination of inlet conditions before coolant blowing was added. Although, the simulation treats the wall fully turbulent and does not model the laminar-turbulent transition the agreement between numerical and experimental values is excellent. This is related to two contrary effects on the boundary layer growth occurring in the experiment (but not in the simulation) that cancel each other out. The tripping device has a thickening influence, whereas the laminar boundary layer growth up to the point of flow transition is weaker when compared to fully turbulent flow. This finding has already been reported by Meinert [19]. Various Air blowing rates from $F = 0.0836\% - 0.5206\%$ were simulated and an excellent agreement to the experiment is found. The effect of a growing injection rate is well captured in the simulations. It is clearly notable that the boundary layer thickness increases and the velocity gradients diminish with rising blowing parameter.

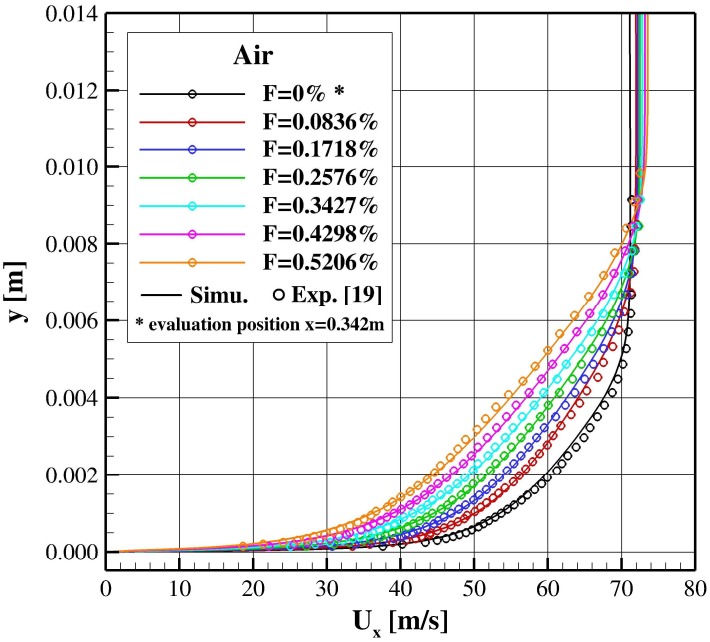

Figure 7: Velocity profiles at $x = 0.442$ m for blowing with Air into a main flow of Air for varying blowing ratio at isothermal conditions.

5.2 Injection of foreign gases at isothermal conditions

Transpiration of the gases Argon and Helium requires the modelling of gas mixtures and species diffusion as described in chapters 2.3 and 2.4. Moreover, the mass inlet boundary condition at the porous wall has to be modelled with special care in order to meet a desired blowing ratio. For the case of foreign gas injection, mass transport does not only take place through convective transport but an additional mass flux due to diffusion occurs. The combination of both yields the total mass flow rate of foreign gas into the main flow and is utilized in the calculation of the blowing ratio $F = (\dot{m}_c/A_c)/(\dot{m}_{hg}/A_{hg})$. Therefore, the so-called Eckert-Schneider boundary condition as described by Schlichting and Gersten [34] was applied to the transpired surface. It assumes that the external component, in our case Air, does not penetrate the wall from which the foreign gas component is transpired. Consequently, the diffusion flux of Air is equal in magnitude and opposite in sign to the area-specific mass flow rate of Air. For our geometry with blowing in y-direction, this leads to

$$j_{2,w} = -\rho_2 \, U_{y,w} = -\rho \, U_{y,w} \, (1 - Y_1) = -j_{1,w} = \rho \, D_{12} \, \frac{\partial Y_1}{\partial y} \quad , \tag{19}$$

where $j_{1,w}$ and $j_{2,w}$ are the diffusion fluxes of foreign gas (subscript '1') and Air main flow (subscript '2') in wall-normal direction. Since the injection of heavy (Argon) or light (Helium) gases changes the density within the

DOI: 10.13009/EUCASS2017-589

boundary layer, the velocity profile does not correctly reproduce the momentum deficit in the wall-near region. Thus, the mass flux density ρU_x is employed for the analysis of foreign gas transpiration.
Figures 8 and 9 display the mass flux density over wall distance for Argon and Helium injection. An excellent agreement between simulation and experiments for Argon and a good agreement for Helium is found. The boundary layer thickening as well as the reduced gradients in comparison to the no-blowing case are well represented. It is notable that even comparatively small injections of Helium change the mass flux density distribution significantly. This is a consequence of Helium's much lower density when compared to Air ($\rho_{Air}/\rho_{He} \approx 7.25$) which decreases the mixture density close to the wall and moreover results in comparatively large transversal velocities. Argon as a heavier gas ($\rho_{Air}/\rho_{Ar} \approx 0.725$) has a reduced effect in this regard.
The presented simulation results of Argon and Helium injection show little deviations to the measured data. Taking into consideration that the experimental results naturally include some measurement uncertainties and are additionally based on analytical diffusion modelling, the agreement is excellent.

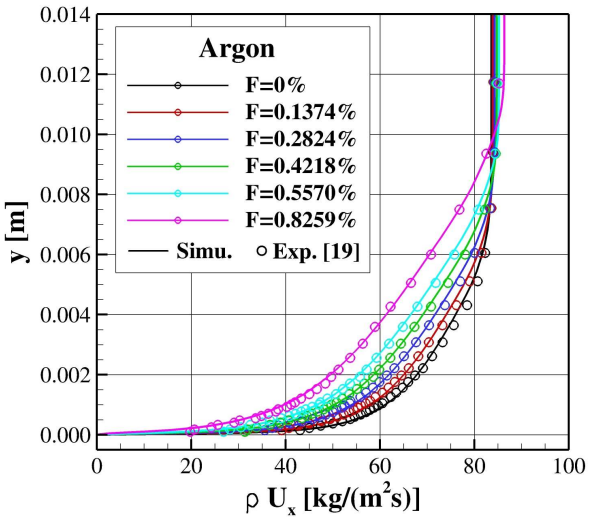

Figure 8: Mass flux density profile at $x = 0.442$ m for boundary layer blowing with Argon into a main flow of Air at isothermal conditions.

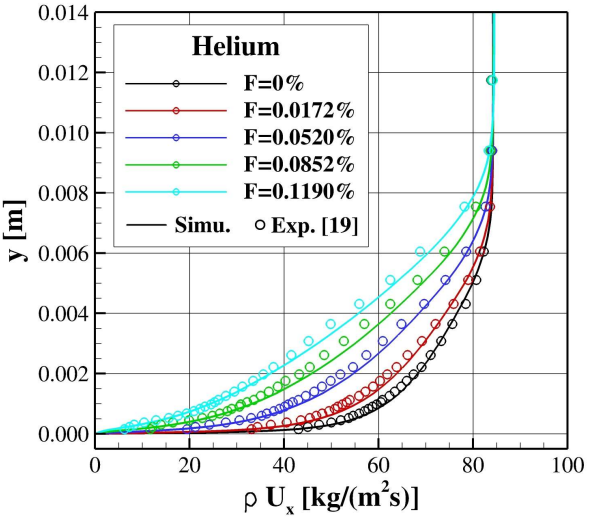

Figure 9: Mass flux density profile at $x = 0.442$ m for boundary layer blowing with Helium into a main flow of Air at isothermal conditions.

5.3 Injection of foreign gases into a heated main flow

Having validated the injection of foreign gases at isothermal conditions, in the following the simulation results for a heated main flow and a transpiration-cooled porous wall are compared to the experimental data by Meinert. For Argon injection the main flow temperature is set to $T_{hg,Ar} = 456$ K, whereas for Helium injection the experiments were performed at higher temperatures yielding $T_{hg,He} = 550$ K. The coolant temperature is set identical to the porous wall temperature which was measured in the experiments. As mentioned before, the thermal state of the channel wall up- and downstream of the sample position is not exactly known. Therefore, the temperatures were set to the porous wall measurements without blowing. Opposed to the isothermal cases, the temperature dependence of fluid properties, e.g. μ and λ, as well as the molecular diffusion coefficient (i.e. $D_{12} \sim T^{1.75}$) has to be considered for the test cases with a heated main flow.
Figures 10 and 11 show the results for the heated test cases of foreign gas injections. In addition to the mass flux density, the temperature profile is given on the second abscissa.

DOI: 10.13009/EUCASS2017-589

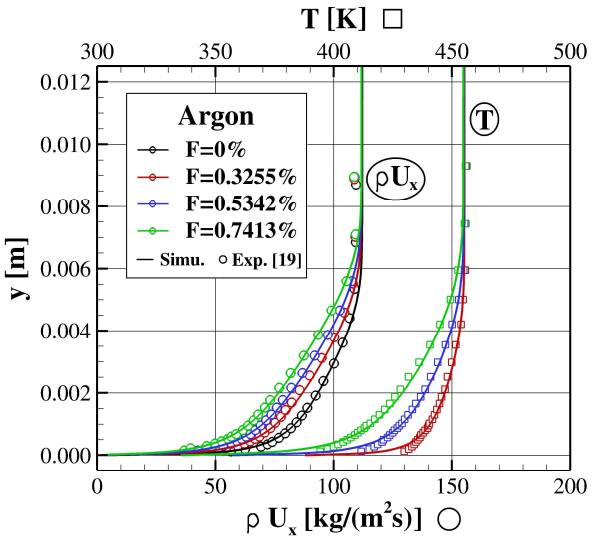

Figure 10: Mass flux density profiles (x_1-axis, symbol ○) and temperature profiles (x_2-axis, symbol □) at $x = 0.342$ m for boundary layer blowing with Argon into a heated main flow of Air.

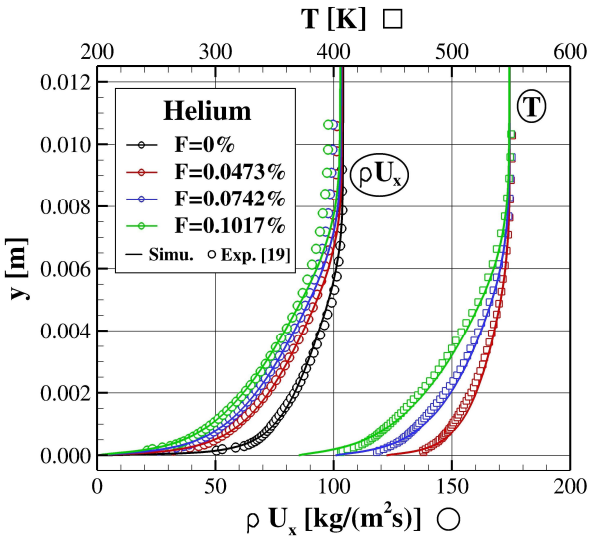

Figure 11: Mass flux density profiles (x_1-axis, symbol ○) and temperature profiles (x_2-axis, symbol □) at $x = 0.442$ m for boundary layer blowing with Helium into a heated main flow of Air.

Again, a very good agreement for the mass flux density is found for both investigated cases. Especially close to the wall, experimental and simulation data coincide nearly perfect, whereas further away from the wall smaller deviations occur. Regarding the temperature distributions, a good agreement is found between experiment and simulation. A clear decrease of temperature gradients close to the wall and a thickening of the temperature boundary layer can be noted for coolant gas injection. Identical to the observed effect for the mass flux density, the injection of Helium shows a stronger influence on the temperature boundary layer than Argon. This is due to the high specific heat capacity of Helium ($c_{p,He}/c_{p,Air} \approx 5$) when compared to Argon ($c_{p,Ar}/c_{p,Air} \approx 0.5$).
From the discussed results, we find that the OpenFOAM solver well reproduces the boundary layer profiles of mass flux density and temperature for coolant gas injection into a heated main flow.

5.4 Wall shear stress and heat transfer analysis

The numerical results discussed so far clearly illustrate the influence of boundary layer blowing which thickens the boundary layer and thereby reduces the velocity and temperature gradients close to the wall. For a detailed analysis, dimensionless parameters for wall shear stress and heat transfer are frequently used, i.e. the skin friction coefficient C_f and the Stanton number St. For our study, we define both parameters as:

$$\frac{C_f}{2} = \frac{\tau_w}{\rho_\infty U_{x,\infty}^2} \quad \text{and} \quad St = \frac{\dot{q}_w}{\rho_\infty c_{p,\infty} U_{x,\infty} (T_\infty - T_w)} \quad . \qquad (20), (21)$$

The wall shear stress $\tau_w = \mu_w \, \partial U_x/\partial y|_w$ and the area-specific wall heat flux $\dot{q}_w = -\lambda_w \, \partial T/\partial y|_w$ are evaluated at the wall for $x = 0.442$ m, whereas the reference values are taken as the corresponding free-stream values (subscript '∞'). For transpiration cooling applications, rather the reduction than the absolute values of skin friction and wall heat flux is of special interest. It can be analysed from the ratio of parameters with and without blowing, i.e. C_f/C_{f0} and St/St_0. The skin friction coefficient without blowing C_{f0} is determined from the OpenFOAM simulation without blowing, for the Stanton number St_0 a correlation for turbulent flow over a flat plate as given by Eckert and Livingood [1] is used:

$$St_0 = 0.037 \, Re_x^{-0.2} \, Pr^{-2/3} \quad . \qquad (22)$$

In figure 12 the ratio of skin friction coefficients with and without transpiration is given for injection of Air, Argon and Helium under isothermal conditions. An analogous diagram for the Stanton number of the heated cases is given in figure 13. In addition to the OpenFOAM results, the analytical / semi-empirical correlations by Kays et al. [18] and Meinert [9] as given by equations (2) and (3) are included in the figures. The dimensionless parameters are evaluated at the axial position $x = 0.442$ m of the investigated channel geometry.

DOI: 10.13009/EUCASS2017-589

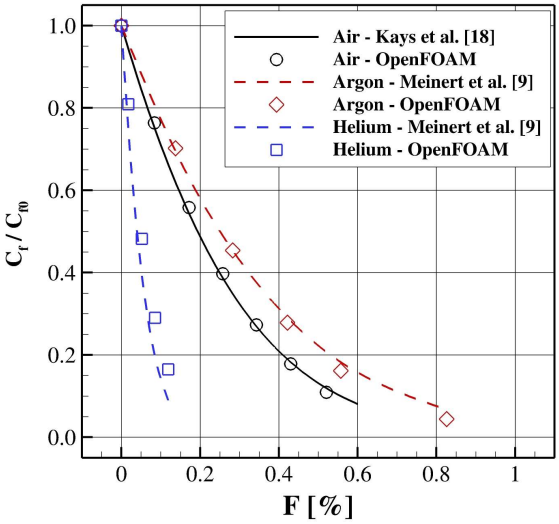

Figure 12: Ratio of skin friction coefficient with and without transpiration over blowing rate for Air, Argon and Helium at isothermal conditions.

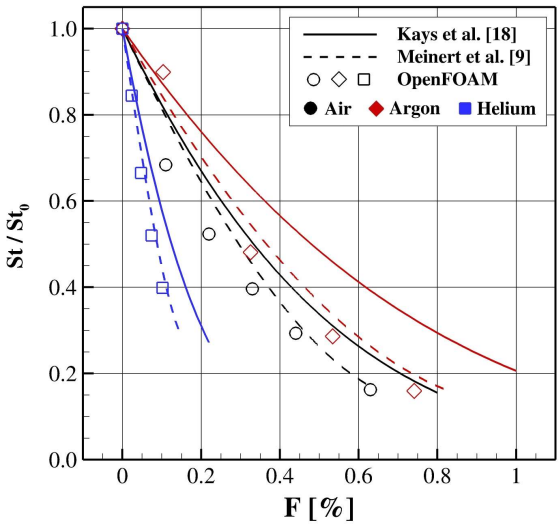

Figure 13: Ratio of Stanton number with and without transpiration over blowing rate for Air, Argon and Helium transpiration into a heated main flow.

Figure 12 clearly illustrates the strong reduction of wall shear stress for mass injection into the boundary layer. Moreover, a pronounced dependency on the coolant fluid properties is found. Light gases such as Helium reduce the skin friction coefficient drastically already at low blowing rates. The highest investigated blowing rate for Argon exhibits a skin friction coefficient close to boundary layer blow-off taking place for $C_f \approx 0$. An excellent agreement between simulation results and correlations is found for the transpiration of Air, Argon and Helium. For blowing with foreign gases the correction $k_M = \left(M_{hg}/M_c\right)^{0.8}$ proposed by Meinert [9] has to be taken into account, though.
Regarding the Stanton number ratio illustrated in figure 13, a distinct reduction of wall heat flux for increased blowing ratios is notable. Again, Helium has a stronger influence when compared to the other gases because of its superior coolant properties. A good agreement is found for the correlation of Meinert et al., whereas the agreement to the correlation of Kays et al. is less.

6. Conclusions

In the given study the simulation of a turbulent channel flow with boundary layer injection is presented. For this purpose, a modified OpenFOAM solver is employed which has been supplemented with models for the calculation of fluid properties of gas mixtures and species diffusion handling. For the purpose of validation, the solver is applied to an experimental test case from literature. Two different injection modelling approaches are explored and compared to each other. The continuous blowing model is selected for further simulations of boundary layer blowing with Air, Argon and Helium. In addition to isothermal test cases, foreign gas injection for heated main flows is investigated which is closer to the original motivation of transpiration cooling. The numerical results are compared to experimentally measured boundary layer profiles for velocity and temperature. Overall, a very good agreement is found between simulation and the experiments by Meinert [19]. Especially for the isothermal test cases with Air and Argon injection, the conformity of results is excellent. The simulation results for the heated test cases with Air, Argon and Helium injection show a good agreement with the measured mass flux density and temperature profiles. All important characteristics such as the thickening of kinematic and thermal boundary layers and the reduction of gradients close to the wall are accurately represented in the simulation. Moreover, the influence of the properties of the injected gas is clearly illustrated. In a last step, the dimensionless parameters C_f and St for wall shear stress and heat transfer are evaluated for the considered coolants and varying blowing ratio. Reductions of both parameters for injection are found which are in good agreement with correlations from literature. Again, the great significance of coolant properties is noted when regarding the excellent cooling performance of Helium. Summing up, an overall good agreement between simulations and experimental data or correlations is found for the investigated validation cases. Thus, our modified OpenFOAM solver performs well in the simulation of foreign gas injection at isothermal and heated conditions and can be applied confidently to the simulation of other transpiration-cooled structures.

DOI: 10.13009/EUCASS2017-589

Acknowledgments

This work was supported by University of Stuttgart and the Helmholtz Alliance within the Helmholtz Young Investigator's Group VH-NG-909 "High Temperature Management in Hypersonic Flight". The corresponding author would like to thank J. Meinert for the fruitful discussions and the contribution of experimental data given in reference [19].

References

[1] Eckert, E. R. G. and N. B. Livingood. 1954. Comparison of Effectiveness of Convection-, Transpiration-, and Film-Cooling Methods with Air as Coolant. *NACA Technical Report 1182*.

[2] Frieß, M., W. Krenkel, R. Kochendörfer, R. Brandt, G. Neuer, and H.-P. Maier. 2005. High temperature materials and hot structures. *In: Jacob, D., Sachs, G., Wagner, S., editors. Basic Research and Technologies for Two-Stage-to-Orbit Vehicles.* Weinheim: Wiley-VCH.

[3] Hald, H., M. Ortelt, I. Fischer, D. Greuel, and O. Haidn. 2005. Effusion cooled CMC rocket combustion chamber. *AIAA/CIRA 13th International Space Planes and Hypersonics Systems and Technologies Conference.* Capua, Italy. AIAA 2005-3229.

[4] Böhrk, H. 2014. Transpiration Cooling at Hypersonic Flight - AKTiV on SHEFEX II. *11th AIAA/ASME Joint Thermophysics and Heat Transfer Conference.* Atlanta, GA. AIAA 2014-2676.

[5] Kuhn, M. and H. Hald. 2008. Application of Transpiration Cooling for Hot Structures. *In: Guelhan, A., editor. RESPACE: Key Technologies for Reusable Space Systems*. ISBN 978-3540778189. Springer.

[6] Darcy, H. 1856. Les fontaines publiques de la ville de Dijon. Victor Dalmont, Paris.

[7] Lage, J. L. 1998. The Fundamental Theory of Flow through Permeable Media from Darcy to Turbulence. *In: Ingham, D. B. and Pop, I., editors. Transport Phenomena in Porous Media*. ISBN 978-0080428437. Pergamon.

[8] Nield, D. A. and A. Bejan. 2006. Convection in Porous Media. 3rd Edition. ISBN 978-1461455417. Springer.

[9] Meinert, J., J. Huhn, E. Serbest, and O. Haidn. 2001. Turbulent Boundary Layers with Foreign Gas Transpiration. *Journal of Spacecraft and Rockets.* Vol. 38(2), pp. 191-198, 2001.

[10] Moffat, R. J. and W. M. Kays. 1968. The Turbulent Boundary Layer on a Porous Plate: Experimental Heat Transfer with Uniform Blowing and Suction. *International Journal of Heat and Mass Transfer.* Vol. 11(10), pp. 1547-1566, 1968.

[11] Kays, W. M. 1971. Heat Transfer to the Transpired Turbulent Boundary Layer. *International Journal of Heat and Mass Transfer.* Vol. 15(5), pp. 1023-1044, 1972.

[12] Bellettre, J., F. Bataille, and A. Lallemand. 1999. A new Approach for the Study of Turbulent Boundary Layers with Blowing. *International Journal of Heat and Mass Transfer.* Vol. 42(15), pp. 2905-2920, 1999.

[13] Schweikert, S., J. von Wolfersdorf, M. Selzer, and H. Hald. 2013. Experimental Investigation on Velocity and Temperature Distributions of Turbulent Cross Flows over Transpiration Cooled C/C Wall Segments. *5th European Conference for Aeronautics and Space Sciences (EUCASS).* Munich, Germany.

[14] Prokein, D., H. Böhrk, and J. von Wolfersdorf. 2015. Analysis of Anisotropy Effects for Transpiration Cooled CMC Leading Edges using OpenFOAM. *20th AIAA International Space Planes and Hypersonic Systems and Technologies Conference*. Glasgow, United Kingdom. AIAA 2015-3552.

[15] Leadon, B. M. and C. J. Scott. 1956. Measurement of Recovery Factors and Heat Transfer Coefficients with Transpiration Cooling in a Turbulent Boundary Layer at M=3 using Air and Helium as Coolants. *No. RR-126. Minnesota University Rosemount Aeronautical Labs.*

[16] Rubesin, M. W. 1954. An Analytical Estimation of the Effect of Transpiration Cooling on the Heat-Transfer and Skin-Friction Characteristics of a Compressible, Turbulent Boundary Layer. *NACA Technical Note 3341*.

[17] Landis, R. B. and A. F. Mills. 1972. The Calculation of Turbulent Boundary Layers with Foreign Gas Injection. *International Journal of Heat and Mass Transfer.* Vol. 15(10), pp. 1905-1932, 1972.

[18] Kays, W. M, M. E. Crawford, and B. Weigand. 2004. Convective Heat and Mass Transfer. 4th Edition. ISBN 978-0071238298. McGraw-Hill. New York.

[19] Meinert, J. 2000. Haftreibung und Wärmeübergang in einer turbulenten Grenzschicht bei Fremdgas-transpiration. TU Dresden. Dissertation. Fortschritt-Berichte VDI, Reihe 7: Strömungstechnik, Nr. 402. ISBN 978-3183402076.

[20] Dunbar, D. I. A. and L. C. Squire. 1971. Correlations of Concentration, Temperature and Velocity Profiles in Compressible Turbulent Boundary Layers with Foreign Gas Injection. *International Journal of Heat and Mass Transfer.* Vol. 14(1), pp. 27-40, 1971.

DOI: 10.13009/EUCASS2017-589

[21] Menter, F. R. 1994. Two-Equation Eddy-Viscosity Turbulence Models for Engineering Applications. *AIAA Journal.* Vol. 32(8), pp. 1598-1605, 1994.
[22] Launder, B. E. and B. I. Sharma. 1974. Application of the Energy-Dissipation Model of Turbulence to the Calculation of Flow near a Spinning Disc. *Letters in Heat and Mass Transfer.* Vol. 1(2), pp. 131-137, 1974.
[23] Wilcox, D. C. 1988. Reassessment of the Scale-Determining Equation for Advanced Turbulence Models. *AIAA Journal.* Vol. 26(11), pp. 1299-1310, 1988.
[24] Menter, F. R., M. Kuntz, and R. Langtry. 2003. Ten Years of Industrial Experience with the SST Turbulence Model. *In: Hanjalić, K., Nagano, Y., Tummers, M. J., editors. Turbulence, Heat and Mass Transfer 4.* ISBN 978-1567001969. Begell House.
[25] Burcat, A., and B. Ruscic. 2005. Third Millenium Ideal Gas and Condensed Phase Thermochemical Database for Combustion with Updates from active Thermochemical Tables. *Argonne National Laboratory Report number ANL-05/20.*
[26] Sutherland, W. 1893. The Viscosity of Gases and Molecular Force. *Philosophical Magazine.* Vol. 36, pp. 507-531, 1893.
[27] White, F. M. 2005. Viscous Fluid Flow. 3rd Edition. ISBN 978-0072402315. McGraw-Hill. New York.
[28] Poling, B. E., J. M. Prausnitz, and J. P. O'Connell. 2001. The Properties of Gases and Liquids. 5th Edition. ISBN 978-0071189712. McGraw-Hill. New York.
[29] Wilke, C. R. 1950. A Viscosity Equation for Gas Mixtures. *The Journal of Chemical Physics.* Vol. 18(4), pp. 517-519, 1950.
[30] Dean, D. E. and L. I. Stiel. 1965. The Viscosity of Nonpolar Gas Mixtures at Moderate and High Pressures." *AIChE Journal.* Vol. 11(3), pp. 526-532, 1965.
[31] Wassiljewa, A. 1904. Wärmeleitung in Gasgemischen. *Physikalische Zeitschrift.* Vol. 5(22), pp. 737-742, 1904.
[32] Mason, E. A. and S. C. Saxena. 1958. Approximate Formula for the Thermal Conductivity of Gas Mixtures. *The Physics of Fluids.* Vol. 1(5), pp. 361-369, 1958.
[33] Tandon, P. K. and S. C. Saxena. 1965. *Appl. Sci. Res.* Vol. 19, 1965.
[34] Schlichting, H. and K. Gersten. 2003. Boundary-Layer Theory. 8th Edition. ISBN 978-3540662709. McGraw-Hill. New York.
[35] Sparrow, E. M., W. J. Minkowycz, E. R. G. Eckert, and W.E. Ibele. 1964. The Effect of Diffusion Thermo and Thermal Diffusion for Helium Injection into Plane and Axisymmetric Stagnation Flow of Air. *Journal of Heat Transfer*. Vol. 86(3), pp. 311-319, 1964.
[36] Anderson, J. D. 1988. Hypersonic and High Temperature Gas Dynamics. ISBN 978-0070016712. McGraw-Hill. New York.
[37] Fuller, E. N., K. Ensley, and J. C. Giddings. 1969. Diffusion of Halogenated Hydrocarbons in Helium. The Effect of Structure on Collision Cross Sections. *The Journal of Physical Chemistry.* Vol. 73(11), pp. 3679-3685, 1969.
[38] Fuller, E. N. and J. C. Giddings. 1965. A Comparison of Methods for Predicting Gaseous Diffusion Coefficients. Journal of Chromatographic Science. Vol. 3(7), pp. 222-227, 1965.
[39] Wagner, A., M. Kuhn, J. M. Schramm, and K. Hannemann. 2013. Experiments on Passive Hypersonic Boundary Layer Control using Ultrasonically Absorptive Carbon–Carbon Material with Random Microstructure. *Experiments in Fluids.* Vol. 54(10), p. 1606, 2013.
[40] Wuest, W. 1969. Strömungsmesstechnik: Lehrbuch für Aerodynamiker, Strömungsmaschinenbauer, Lüftungs- und Verfahrenstechniker ab 5. Semester. ISBN 978-3663045328. Vieweg.
[41] Issa, R. I. 1986. Solution of the Implicitly Discretised Fluid Flow Equations by Operator-Splitting. *Journal of Computational Physics.* Vol. 62(1), pp. 40-65, 1986.
[42] Versteeg, H. K. and W. Malalasekera. 2007. An Introduction to Computational Fluid Dynamics: The Finite Volume Method. 2nd edition. ISBN 978-0131274983. Pearson.